Fission yeast paxillin contains two Cdc15 binding motifs for robust recruitment to the cytokinetic ring

Chloe E. Snider†, Rahul Bhattacharjee, Maya G. Igarashi, and Kathleen L. Gould*
Department of Cell and Developmental Biology, Vanderbilt University School of Medicine, Nashville, TN 37232

ABSTRACT **The F-BAR protein Cdc15 mediates attachment of the cytokinetic ring (CR) to the plasma membrane and is essential for cytokinesis in *Schizosaccharomyces pombe*. While its N-terminal F-BAR domain is responsible for oligomerization and membrane binding, its C-terminal SH3 domain binds other partners at a distance from the membrane. We previously demonstrated that the essential cytokinetic formin Cdc12, through an N-terminal motif, directly binds the cytosolic face of the F-BAR domain. Here, we show that paxillin-like Pxl1, which is important for CR stability, contains a motif highly related to that in formin Cdc12, and also binds the Cdc15 F-BAR domain directly. Interestingly, Pxl1 has a second site for binding the Cdc15 SH3 domain. To understand the importance of these two Pxl1-Cdc15 interactions, we mapped and disrupted both. Disrupting the Pxl1-Cdc15 F-BAR domain interaction reduced Pxl1 levels in the CR, whereas disrupting Pxl1's interaction with the Cdc15 SH3 domain, did not. Unexpectedly, abolishing Pxl1-Cdc15 interaction greatly reduced but did not eliminate CR Pxl1 and did not significantly affect cytokinesis. These data point to another mechanism of Pxl1 CR recruitment and show that very little CR Pxl1 is sufficient for its cytokinetic function.**

Monitoring Editor
Rong Li
Johns Hopkins University and National University of Singapore

Received: Nov 12, 2021
Revised: Jan 13, 2022
Accepted: Jan 26, 2022

INTRODUCTION

Many eukaryotes, including the fission yeast *Schizosaccharomyces pombe* build and constrict an actin- and myosin-based cytokinetic ring (CR) to bring together opposing membranes and complete cell division (Cheffings *et al.*, 2016; Gould, 2016). Studies utilizing *S. pombe* have revealed a complete "parts list" of ~39 proteins in the CR, many of which are conserved in higher eukaryotes (PomBase; Wood *et al.*, 2012). The amount of each protein in the CR, the order in which the proteins arrive at the division site, and the nanoscale organization of the proteins within the CR have all been characterized (Pollard and Wu, 2010; Goyal *et al.*, 2011; Cheffings *et al.*, 2016; Rincon and Paoletti, 2016; McDonald *et al.*, 2017; Mangione and Gould, 2019). The complex relationships between these components, how they are regulated, and how they work together to form a functional contractile unit are not fully understood.

S. pombe paxillin-like Pxl1 was identified as a conserved CR protein based on sequence similarity to *Saccharomyces cerevisiae* Pxl1 and human paxillin and consists of a proline-rich N-terminus and three C-terminal LIM domains (Ge and Balasubramanian, 2008; Pinar *et al.*, 2008). Approximately 70 human genes encode proteins containing LIM domains, some of which are associated with focal adhesions, cell–cell adhesions, and stress fibers (Smith *et al.*, 2014; Winkelman *et al.*, 2020). Consistent with their function at actin-rich structures, recent studies have shown that several LIM domains, including ones in Pxl1, directly bind tensed F-actin (Sun *et al.*, 2020; Winkelman *et al.*, 2020). Although the precise function of *S. pombe* Pxl1 at the CR is not completely understood, it is thought to behave as a scaffold, similar to human paxillin at focal adhesions (Turner, 2000; Schaller, 2001; López-Colomé *et al.*, 2017). Indeed, Pxl1 associates with and recruits the protein phosphatase calcineurin to the CR (Martín-García *et al.*, 2018). Cells lacking Pxl1 exhibit a variety of defects indicating CR instability, including CR sliding from the cell center toward one of the cell ends, CR splitting, and prolonged duration of constriction compared with wild-type cells

This article was published online ahead of print in MBoC in Press (http://www.molbiolcell.org/cgi/doi/10.1091/mbc.E21-11-0560) on February 2, 2022.

†Present address: Department of Pathology and Laboratory Medicine, Children's Hospital of Philadelphia Research Institute, Philadelphia, PA 19104.

*Address correspondence to: Kathleen L. Gould (kathy.gould@vanderbilt.edu).

Abbreviations used: CR, cytokinetic ring; mNG, mNeonGreen; SPB, spindle pole body.

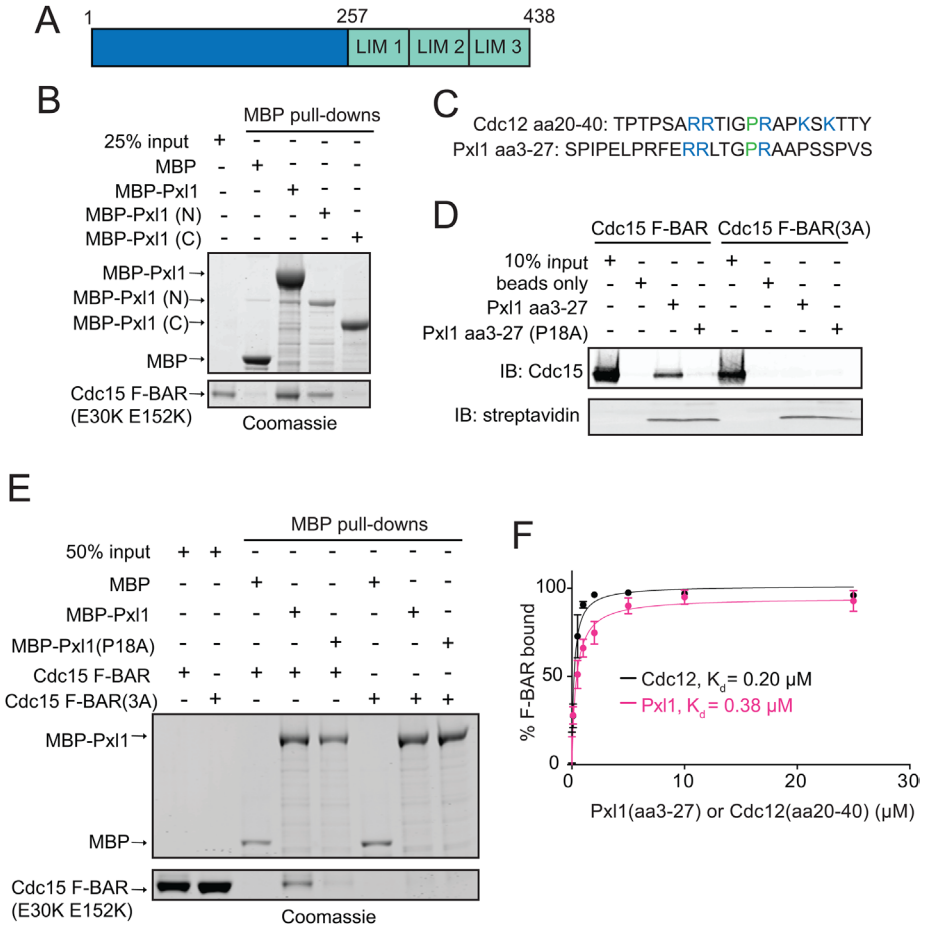

FIGURE 1: Pxl1 binds the cytosolic face of the Cdc15 F-BAR domain. (A) Schematic of Pxl1 to scale with residues at fragment borders indicated. (B) In vitro binding assay with indicated Cdc15 F-BAR domain constructs and MBP-Pxl1 fusions. Proteins associated with amylose resin after the binding reaction were analyzed by SDS–PAGE and Coomassie blue staining. Pxl1 N = residues 1–257, Pxl1 C = residues 238–438. (C) F-BAR binding motifs in Cdc12 and Pxl1. The prolines critical for interaction are highlighted in green and basic residues are in blue. (D) In vitro binding assay with biotinylated Pxl1 peptides and Cdc15 F-BAR domains. Proteins associated with streptavidin resin after the binding reaction were separated by SDS–PAGE and analyzed by immunoblotting Cdc15 or streptavidin. (E) In vitro binding assay with MBP-Pxl1 wild-type and P18A with indicated Cdc15 F-BAR domain constructs analyzed by SDS–PAGE and Coomassie blue staining. (F) Binding curves for Pxl1 peptide (residues 3–27, magenta) and Cdc12 peptide (residues 20–40, black) binding to wild-type Cdc15 F-BAR domain. Dissociation constants calculated from three experiments are Cdc12: $K_d = 0.20 \pm 0.08$; Pxl1: $K_d = 0.38 \pm 0.04$. Error bars represent standard error of the mean (SEM).

(Ge and Balasubramanian, 2008; Pinar *et al.*, 2008; Cortés *et al.*, 2015). *S. pombe* is a walled organism, therefore new cell wall material must be deposited at the division site to form the division septum and complete cytokinesis. Because septation is coupled to CR constriction, *pxl1Δ* also displays abnormal cell wall phenotypes such as off-center septation, formation of multiple septa, and abnormally thick cell walls (Cortés *et al.*, 2015). These morphological defects are similar to those described for deletion of the gene encoding the calcineurin catalytic subunit Ppb1, which does not localize to the CR in *pxl1Δ* cells, suggesting that scaffolding calcineurin at the CR may be the major function of Pxl1 (Martín-García *et al.*, 2018).

However, Pxl1 is not sufficient for CR calcineurin recruitment. Even though Pxl1 localizes normally to the CR, calcineurin is absent from the CR in an internal deletion mutant of the essential F-BAR protein and CR anchor Cdc15 (*cdc15Δ2*; Mangione *et al.*, 2019). Further, Cdc15 is required for both Pxl1 and calcineurin localization to the CR (Snider *et al.*, 2020). Cdc15 has an N-terminal membrane-binding F-BAR domain, a medial predicted intrinsically disordered region (IDR), and a C-terminal SH3 domain. During interphase, Cdc15 is hyperphosphorylated on residues within the IDR, which inhibits Cdc15's membrane and protein binding activities; dephosphorylation of Cdc15 upon mitotic entry allows its oligomerization, membrane binding, and interaction with Pxl1 and other CR components (Roberts-Galbraith *et al.*, 2010; Kettenbach *et al.*, 2015; Bhattacharjee *et al.*, 2020). The Cdc15 SH3 domain is thought to have a role in Pxl1 accumulation during septum formation by directly interacting with Pxl1 (Roberts-Galbraith *et al.*, 2009; Cortés *et al.*, 2015). However, the Cdc15 SH3 domain alone is insufficient to bind full-length Pxl1 in vitro, as a portion of the adjacent IDR is also required (Bhattacharjee *et al.*, 2020). Pxl1 also directly binds the Cdc15 F-BAR domain, which in turn binds the plasma membrane (Snider *et al.*, 2020). How Pxl1 is able to engage both the membrane-proximal Cdc15 F-BAR domain and the Cdc15 C-terminus, which in cells occupy spatially separate regions of the CR (McDonald *et al.*, 2017), is not clear.

Here, we explored the molecular underpinnings of Cdc15-Pxl1 interactions and their role in Pxl1 and calcineurin CR localization. We defined the Pxl1 motifs responsible for the Cdc15 F-BAR and SH3 domain interactions and demonstrated that mutation of these motifs renders Pxl1 unable to bind Cdc15. Cells lacking either Cdc15 F-BAR interaction or both Cdc15 F-BAR and SH3 interaction with Pxl1 had significantly reduced levels of Pxl1 and calcineurin at the division site. We propose that Pxl1 and Cdc15 work together to create a binding platform for calcineurin at the CR, which promotes accurate completion of cytokinesis.

RESULTS AND DISCUSSION

Pxl1 contains an N-terminal F-BAR binding motif

We first defined precisely how Pxl1 engages with the Cdc15 F-BAR domain. We found that the N-terminus of Pxl1 (MBP-Pxl1-N; residues 1–257), but not the LIM-domain-containing C-terminus (MBP-Pxl1-C; residues 238–end), bound the Cdc15 F-BAR domain (Figure 1, A and B). In Pxl1-N, we identified a motif (residues 3–27) with high sequence similarity to the motif of the cytokinetic formin Cdc12 that interacts with the Cdc15 F-BAR domain (Figure 1C; Willet *et al.*, 2015). A peptide consisting of this motif, Pxl1 (residues 3–27), bound the Cdc15 F-BAR domain, but not the Cdc15(3A) mutant F-BAR domain that disrupts Pxl1 binding (Figure 1D; Snider *et al.*, 2020). Within the Cdc12 motif, P31 is required for F-BAR interaction (Willet *et al.*, 2015). When the analogous proline in Pxl1 (P18; Figure 1C, green) was mutated to alanine in the context of the F-BAR

binding motif peptide (residues 3–27; Figure 1D) or in the context of full-length MBP-Pxl1 (Figure 1E), Pxl1(P18A) did not interact with the Cdc15 F-BAR domain. Peptides containing the F-BAR binding motifs of Cdc12 and Pxl1 bound the Cdc15 F-BAR domain with similar affinities (Figure 1F), consistent with the sequence similarity of the two motifs. Together, these results indicate that Pxl1, like Cdc12, contains an N-terminal motif that binds the cytosolic face of the Cdc15 F-BAR domain.

A single Pxl1 PxxP motif is necessary and sufficient for binding the Cdc15 C-terminus

The Cdc15 SH3 domain is insufficient to bind full-length Pxl1 because a portion of the IDR is also required. Nevertheless, mutation of the SH3 domain (W903S) to abolish binding to PxxP motifs significantly reduced Pxl1 binding to Cdc15C (residues 441–end; Bhattacharjee *et al.*, 2020). This led to the hypothesis that one or more of the six PxxP motifs in Pxl1 (Figure 2A) are important for binding to Cdc15C. We found that mutation of all six Pxl1 PxxP motifs to alanine (AxxA$^{1–6}$) substantially reduced binding of Pxl1 to Cdc15C, similar to the effect of Cdc15(W903S) (Figure 2B). We previously reported that smaller Cdc15C fragments contained the Pxl1 binding region (Bhattacharjee *et al.*, 2020), thus we used Cdc15 residues 600–end, hereafter termed Cdc15C1, to determine which Pxl1 PxxP motif(s) is important for Cdc15 interaction. First, we confirmed that Cdc15C1 bound Pxl1 similarly to Cdc15C (Figure 2C). Next, we tested mutations of three motifs at a time (AxxA$^{1–3}$ or AxxA$^{4–6}$), which were clustered in the linear protein sequence (Figure 2A). MBP-Pxl1 (AxxA$^{1–3}$) bound Cdc15C1 similarly to wild type, while MBP-Pxl1 (AxxA$^{4–6}$) did not bind Cdc15C1 (Supplemental Figure S1A). Mutation of the sixth PxxP alone (AxxA^{6}) or in combination with mutation of the fourth or fifth motifs (AxxA^{4,6} or AxxA^{5,6}) reduced Cdc15C1 binding comparable to AxxA$^{1–6}$ (Supplemental Figure S1, A and B), indicating that the sixth Pxl1 motif is responsible for interaction with Cdc15C1. Not surprisingly, this motif is the only PxxP that conforms to the K/RXLPXΦP motif characteristic of Cdc15 SH3 ligands (Supplemental Figure S1C; Ren *et al.*, 2015). We found that a synthetic peptide containing the PxxP^{6} motif (Pxl1 residues 177–188) bound Cdc15C1 or the Cdc15-SH3 domain, whereas an AxxA variant of the peptide did not (Figure 2D). The K_d value for the PxxP^{6} peptide binding with Cdc15C1 was 1.9 ± 0.3 μM, which is within the typical range measured for other SH3-PxxP interactions (Figure 2E; Feng *et al.*, 1994; Yu *et al.*, 1994; Teyra *et al.*, 2017). Thus, a canonical Cdc15 SH3 interaction with a Pxl1 PxxP motif occurs, at least in vitro.

Pxl1 has two binding interfaces for binding full-length Cdc15

We next tested whether the P18-containing motif that binds the Cdc15 F-BAR (Figure 1) and the PxxP^{6} motif (Figure 2) are the only two Pxl1 determinants necessary to bind full-length Cdc15. As full-length Cdc15 can only be purified from bacteria in its hyperphosphorylated form, Flag-Cdc15 was produced by co-expression with the DRYK kinase Pom1 (Bhattacharjee *et al.*, 2020). The *cdc15* construct also contained the *E30K* and *E152K* mutations to prevent F-BAR domain oligomerization that complicates pull-down experiments (McDonald *et al.*, 2015). Because phosphorylation inhibits Pxl1 binding (Bhattacharjee *et al.*, 2020), purified Cdc15 was treated or not with lambda phosphatase before being combined with MBP, MBP-Pxl1, or MBP-Pxl1 variants in binding reactions. We found that hyperphosphorylated Cdc15 did not appreciably bind any form of Pxl1 (Figure 3A) as observed previously (Bhattacharjee *et al.*, 2020). Both the P18A mutant and the AxxA^{6} mutant bound less dephosphorylated Cdc15 than wild-type Pxl1 (Figure 3A). Binding of the Pxl1 double mutant (P18A + AxxA^{6}) to dephosphorylated Cdc15 was substantially reduced (Figure 3A), indicating that these two Pxl1 motifs constitute the major determinants of Cdc15 association.

In a reciprocal set of experiments, we tested whether the F-BAR and SH3 domains were the primary determinants within Cdc15 for binding Pxl1. We produced a series of full-length Flag-Cdc15(E30K E152K) constructs designed to disrupt Pxl1 binding sites in the F-BAR domain (3A; Snider *et al.*, 2020), the C-terminus (W903S; Bhattacharjee *et al.*, 2020), or both (3A + W903S) and then treated or not with lambda phosphatase. MBP-Pxl1 bound dephosphorylated Flag-Cdc15, Flag-Cdc15(3A), and Flag-Cdc15(W903S) (Figure 3B), indicating that Pxl1 can interact with the F-BAR domain when the C-terminal binding site is compromised and vice versa. MBP-Pxl1 did not appreciably interact with the double mutant Cdc15(3A + W903S) in either its hyper- or hypo-phosphorylated form (Figure 3B), indicating that disruption of both the F-BAR domain and C-terminal binding sites eliminates Cdc15-Pxl1 interaction in vitro.

Pxl1 interaction with the Cdc15 F-BAR domain is required for its robust localization to the CR

To assay the effects of disrupting Pxl1-Cdc15 interaction in vivo, we integrated *pxl1(P18A)*, *pxl1(AxxA^{6})*, and *pxl1(P18A+AxxA^{6})* with an N-terminal mNeonGreen (mNG) tag at the endogenous *S. pombe pxl1* locus. We found that mNG-Pxl1(P18A) was present at much reduced levels in mature CRs compared with mNG-Pxl1 (Figure 4, A and C) and its arrival to the CR appeared delayed, possibly due to reduced levels making detection more difficult (Supplemental Figure S1, D and E). Unexpectedly, mNG-Pxl1(AxxA^{6}) was present at wild-type levels in the CR, and there was no additive effect when Pxl1 mutations disrupting Cdc15 F-BAR and C-terminus binding were combined (Figure 4, A and C). These results indicate that the SH3 domain interaction does not appreciably influence Pxl1 CR recruitment and that Pxl1 binding to the F-BAR domain is the primary means of concentrating Pxl1 at the division site in vivo.

Pxl1 is required to recruit calcineurin to the CR (Martín-García *et al.*, 2018). As expected, calcineurin levels (Ppb1-mNG) were reduced in *pxl1(P18A)* and *pxl1(P18A+AxxA^{6})* but not in *pxl1(AxxA^{6})* (Figure 4, B and D). This parallels previous findings in which a potential calcineurin docking motif (PxIxIT) in Pxl1 located at residues 181–186 (PTLPLQ), which includes PxxP^{6}, was mutated without affecting calcineurin levels at the CR (Martín-García *et al.*, 2018). Despite the significant reduction of Pxl1 and calcineurin levels in the CR, *pxl1(P18A)* and *pxl1(P18A+AxxA^{6})* cellular morphology and septa formation resembled wild type (Supplemental Figure S2, A–C), suggesting that only a small amount of Pxl1 and calcineurin in the CR are sufficient to perform their functions. These results also suggest that Pxl1 has a CR partner besides Cdc15 that helps to recruit it or that the Pxl1(P18A) mutant retains some ability to bind the Cdc15 F-BAR in vivo.

To assay whether the *pxl1* mutants had defects under suboptimal growth conditions, we analyzed their growth at different temperatures, in low-dose latrunculin A (LatA), and in combination with six cytokinesis mutants. We found no evidence of sensitivity to temperature or LatA and observed no negative genetic interactions nor significant suppression (Supplemental Figure S2D). To rigorously test whether the *pxl1* mutants affect cytokinesis progression, we performed time-lapse imaging using Rlc1-mCherry as a CR marker and Sad1-mCherry as a spindle pole body (SPB) marker. We found that strains containing the *pxl1-18A* mutation were modestly delayed in constriction (Supplemental Figure S3A), a result consistent with the reduced CR levels (Cortés *et al.*, 2015).

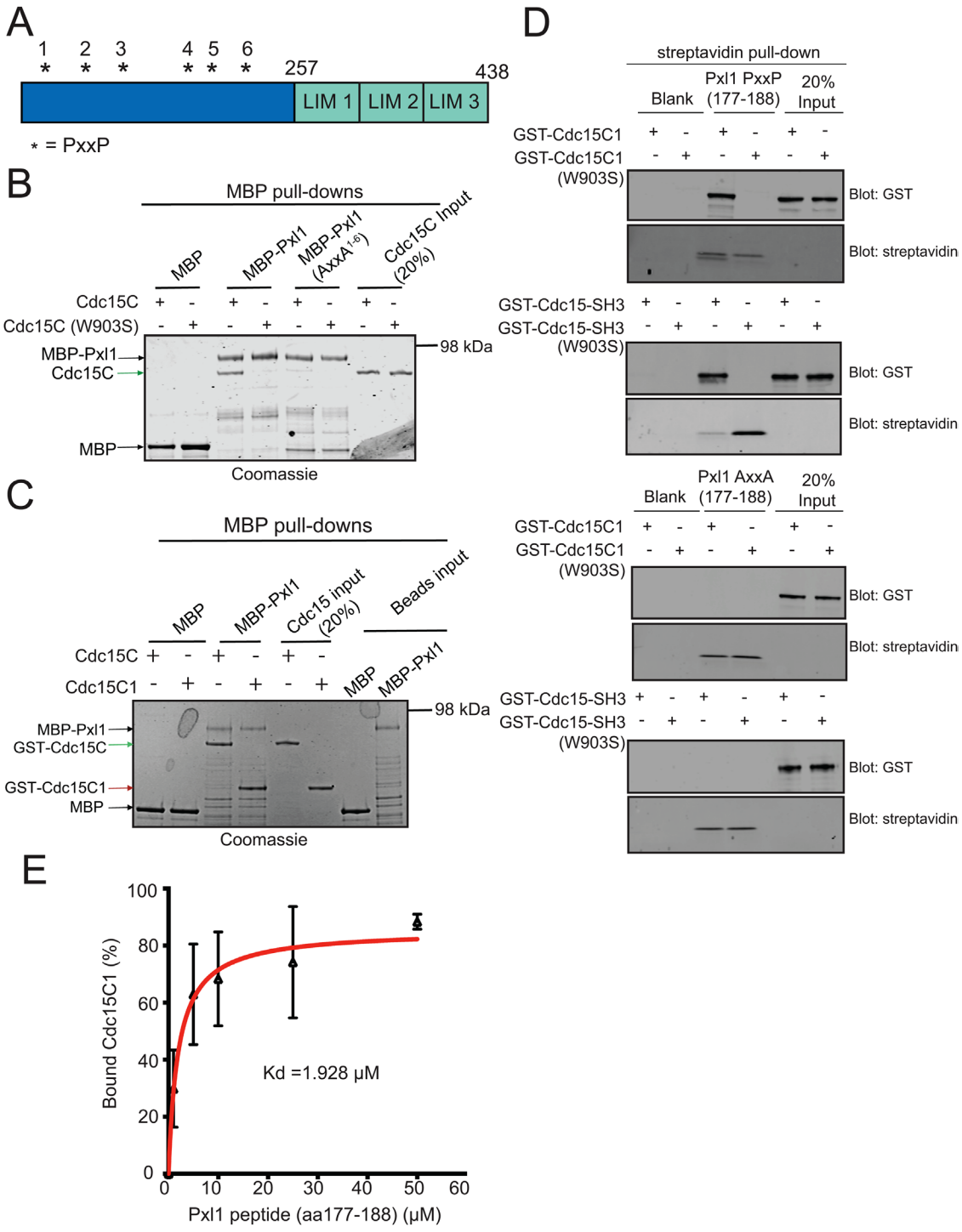

FIGURE 2: A single Pxl1 PxxP motif is necessary and sufficient for Cdc15C binding. (A) Schematic of Pxl1 with position of PxxP motifs indicated by asterisks. (B, C) In vitro binding assays with Cdc15C (residues 441–end) or Cdc15C1 (residues 600–end) and indicated MBP-Pxl1 variants. The binding reactions were analyzed by SDS–PAGE and Coomassie blue staining. (D) In vitro binding assays with biotin-labeled Pxl1 peptides and GST-Cdc15C1, GST-Cdc15C1(W903S), GST-Cdc15-SH3, or GST-Cdc15-SH3(W903S). Proteins bound to the streptavidin resin were analyzed by SDS–PAGE followed by immunoblotting. (E) Binding curves for Pxl1 peptide (aa 177–188) binding to Cdc15C1. The dissociation constant, calculated from three experiments is indicated. Error bars represent SEM.

Pxl1 does not interact with other F-BAR domains

Although certain F-BAR domains can substitute for the Cdc15 F-BAR domain to support cell viability, they have severe morphological and cytokinetic defects, similar to *pxl1*Δ and *ppb1*Δ (Yoshida *et al.*, 1994; Lu *et al.*, 2002; Ge and Balasubramanian, 2008; Pinar *et al.*, 2008; Martín-García *et al.*, 2018; Mangione *et al.*, 2019). We reasoned that this may be due to an inability of the non-Cdc15 F-BAR domains to bind Pxl1 and recruit it to the CR. To test this, we performed binding assays with the Pxl1 peptide (residues 3–27) and two F-BAR domains that can substitute for the essential function of

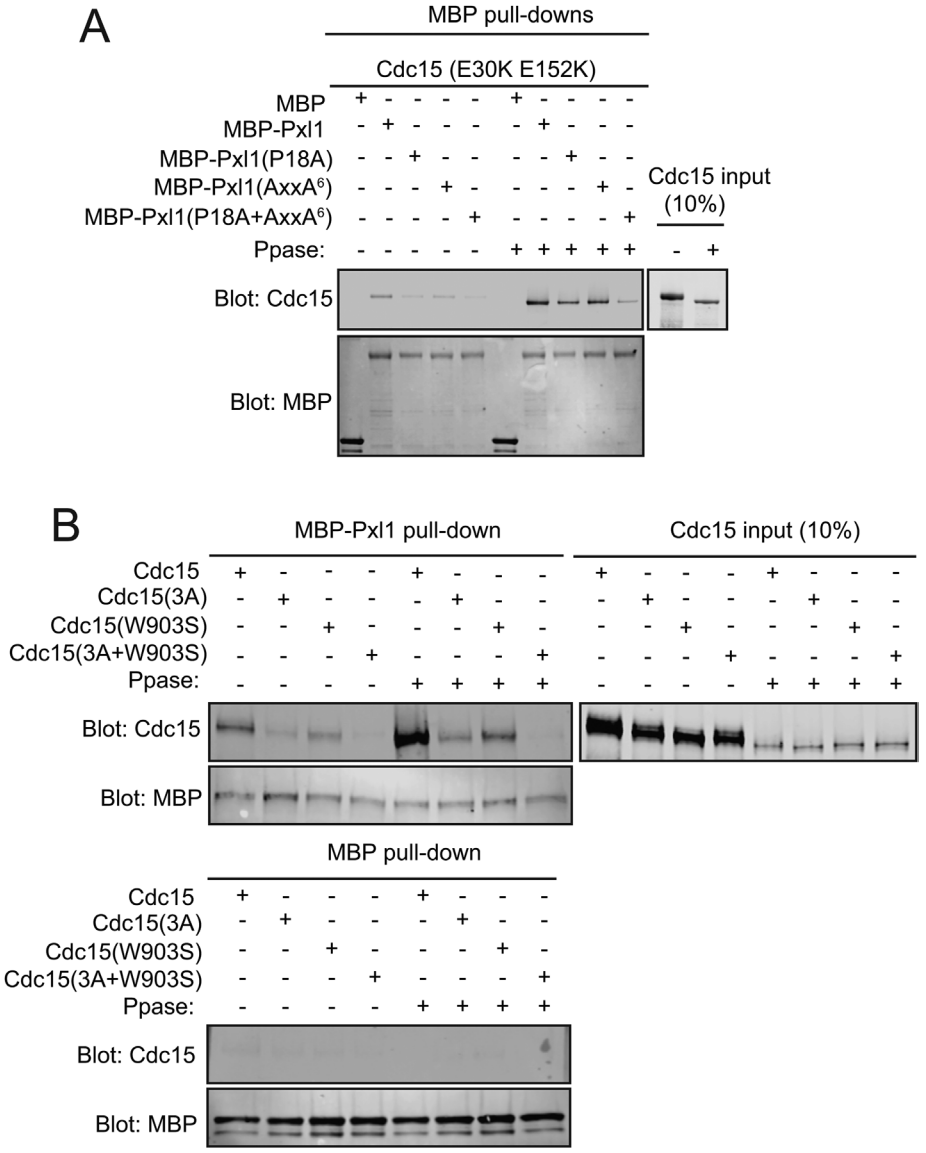

FIGURE 3: The Cdc15 F-BAR domain and C-terminus contribute to Pxl1 interaction in vitro. (A) In vitro binding assays of MBP-Pxl1 variants with full-length Cdc15 (E30K E152K) treated or not with λ-phosphatase (PPase) were analyzed by SDS–PAGE followed by immunoblotting (IB) with anti-Cdc15 and anti-MBP antibodies. (B) In vitro binding assays of MBP-Pxl1 with the indicated full-length Flag-Cdc15 proteins treated or not with λ-PPase were analyzed by SDS–PAGE followed by IB with anti-Cdc15 and anti-MBP antibodies.

the Cdc15 F-BAR domain (Mangione *et al.*, 2019). The Pxl1 peptide bound the Cdc15 F-BAR but not the *S. pombe* Imp2 F-BAR domain or human GAS7 F-BAR domain (Figure 5A). Consistent with this result, there was no detectable mNG-Pxl1 at CRs in cells expressing the chimeric proteins in which the Cdc15 F-BAR domain had been replaced with that of Imp2 or GAS7 at the endogenous *cdc15* locus. While 100% of 89 CRs marked by Cdc15 contained mNG-Pxl1, 0% of 26 CRs in *imp2-cdc15* and 3% of 31 CRs in *GAS7-cdc15* cells had detectable mNG-Pxl1 (Figure 5B), results mirroring what happens when the Pxl1 binding site in the Cdc15 F-BAR is mutated (Snider *et al.*, 2020). Furthermore, these results substantiate that Pxl1 interaction with the Cdc15 SH3 domain is not sufficient to support Pxl1 CR recruitment.

In conclusion, we have identified and characterized multivalent interactions between Pxl1 and the F-BAR protein Cdc15. We previously reported that Pxl1 and formin Cdc12 bind the same patch on the cytosolic face of the Cdc15 F-BAR domain (Snider *et al.*, 2020). Here, we found that Pxl1 contains a Cdc15 F-BAR binding motif highly related to the one within Cdc12 (Willet *et al.*, 2015). While this raises the possibility that Cdc12 and Pxl1 compete for binding the Cdc15 F-BAR, Cdc15 is significantly more abundant than the sum of both (Wu and Pollard, 2005), and as predicted from these data, the same amount of Cdc12-mNG was present in the CR of *pxl1-P18* cells as in wild type (Supplemental Figure S3, B and C). Other F-BAR domains in both yeast and humans have direct binding partners (Kostan *et al.*, 2014; Yao *et al.*, 2014; Begonja *et al.*, 2015; Stanishneva-Konovalova *et al.*, 2016; Oh *et al.*, 2017; Garabedian *et al.*, 2018; Liu *et al.*, 2019; Snider *et al.*, 2021), but the specific sequence determinants required for F-BAR interaction are unknown. Based on the binding specificity of Pxl1 for the Cdc15 F-BAR, it is likely that each F-BAR domain has unique interaction motifs and partners that contribute to functional specificity, in contrast to their common ability to interact with the membrane.

Pxl1 also interacts with the Cdc15 C-terminus (Pinar *et al.*, 2008; Roberts-Galbraith *et al.*, 2009; Martín-García *et al.*, 2018; Bhattacharjee *et al.*, 2020). Our previous work showed that in vitro, the Cdc15 SH3 domain alone fails to bind full-length Pxl1 and a part of the Cdc15 IDR is also required (Bhattacharjee *et al.*, 2020). Furthermore, a mutation in the Cdc15 SH3 domain significantly reduces binding to full-length Pxl1 suggesting that the SH3 domain is necessary but not sufficient to support this interaction (Bhattacharjee *et al.*, 2020). In this study, we found that Pxl1's sixth PxxP motif is responsible for interaction with the Cdc15 SH3 domain. Taken together, these results raise the intriguing possibility that a region in full-length Pxl1 blocks access of the Cdc15 SH3 domain to Pxl1 PxxP⁶ and that some portion of the Cdc15 IDR domain is required to allow this interaction to occur.

Considering that the Cdc15 F-BAR domain and SH3 domain occupy spatially distinct regions within the CR before constriction (McDonald *et al.*, 2017), it remains an open question whether Pxl1 engages both the F-BAR and SH3 domains simultaneously, or whether Pxl1 binds the two domains separately at distinct times. Additionally, it is not known whether the mode in which Cdc15 and Pxl1 engage with one another influences their ability to scaffold calcineurin. This work highlights the complexity of the multivalent protein–protein interactions within the CR and serves as a key step in understanding how Pxl1 and Cdc15 form the binding platform required for calcineurin's crucial signaling roles in cytokinesis.

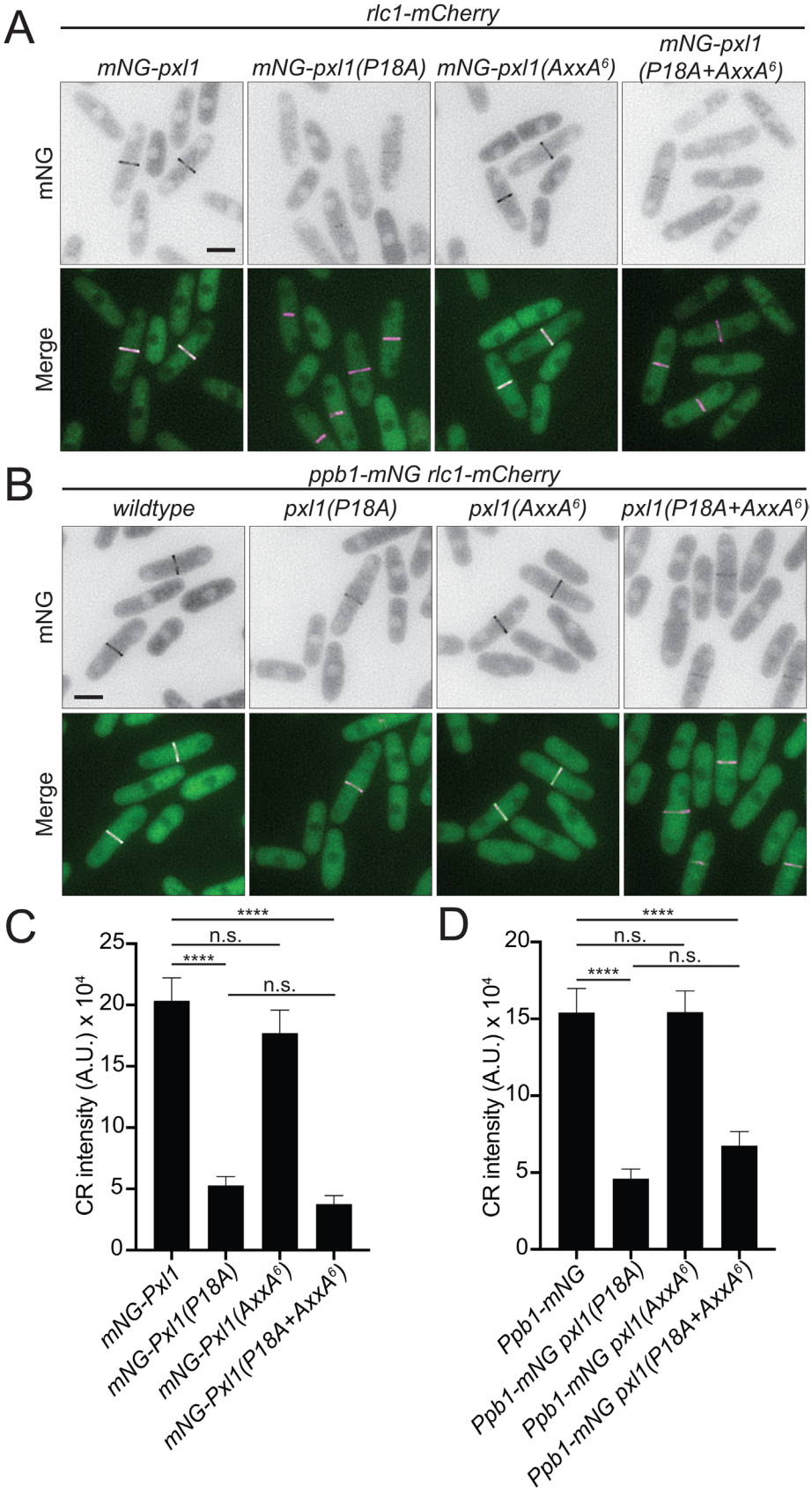

FIGURE 4: Interaction with the Cdc15 F-BAR domain promotes Pxl1 CR localization. (A) Live-cell imaging of indicated *mNG-pxl1 rlc1-mCherry* strains. (B) Live-cell imaging of indicated *ppb1-mNG rlc1-mCherry* strains expressing the indicated *pxl1* alleles. (C) Quantification of CR intensity of cells from A. $n \geq 30$ cells (*mNG-pxl1* vs. *mNG-pxl1(AxxA⁶)*, $p = 0.56$; *mNG-pxl1(P18A)* vs. *mNG-pxl1(P18A+AxxA⁶)*, $p = 0.87$). (D) Quantification of CR intensity of cells from B. $n \geq 45$ cells. ****, $p \leq 0.0001$; one-way ANOVA with Tukey's post hoc test for multiple comparisons; n.s. = not significant (*ppb1-mNG* vs. *ppb1-mNG pxl1(AxxA⁶)*, $p > 0.99$; *ppb1-mNG pxl1(P18A)* vs. *ppb1-mNG pxl1(P18A+AxxA⁶)*, $p = 0.57$). Scale bars, 5 µm. Error bars represent SEM.

MATERIALS AND METHODS

Request a protocol through *Bio-protocol*.

Yeast methods

S. pombe strains used in this study (Supplemental Table S1) were grown in yeast extract (YE) media. For serial dilution growth assay, cells were grown in liquid YE at 25°C. Three 10-fold serial dilutions starting at 4×10^6 cells/ml of each strain were made and 3 µl of each dilution were spotted onto YE agar plates. To define sensitivity of the strains to LatA, the serial dilutions were plated on YE plates in the presence of 0.20 µM LatA (Focus Biomolecules; Cat. #10-2254) or dimethyl sulfoxide (DMSO). Plates with DMSO or LatA were incubated at 32°C and for the rest of the growth assays, at other indicative temperatures for 2–5 d, and then colonies were imaged with a scanner.

Protein purification

F-BAR domains were produced as 6xHis fusions in *Escherichia coli* Rosetta2 (DE3)pLysS cells. Bacteria were grown to log phase in terrific broth, and protein expression was induced overnight at 17°C with 0.1 mM isopropyl β-D-1-thiogalactopyranoside (IPTG; Fisher Scientific; BP1755). Cells were then resuspended in 50 mM Tris, pH 8.0, 300 mM NaCl, 0.1% NP-40, 5 mM 2-mercaptoethanol with 200 µg/ml lysozyme (Sigma-Aldrich; L6876) and lysed by sonicating three times for 30 s, with at least a 30-s pause between sonications (Sonic Dismembrator Model F60, Fisher Scientific; power 15 W). Lysate was then cleared by centrifugation and incubated with cOmplete His-Tag resin (Roche) for 2 h at 4°C. Beads were then washed three times in lysis buffer, and His-tagged protein was eluted in lysis buffer with the addition of 200 mM imidazole. Eluted His-tagged GAS7 F-BAR domain was dialyzed overnight against 50 mM Tris, pH 8.0, 300 mM NaCl, 2 mM DTT, then concentrated with Amicon Ultracentrifugal Filters (EMD Millipore). For Cdc15 and Imp2 F-BAR domains, the 6xHis tag was cleaved from the eluted protein by adding thrombin (2U/µl) at 1:100 for 2 h at room temperature (RT). Cdc15 F-BAR domain was further

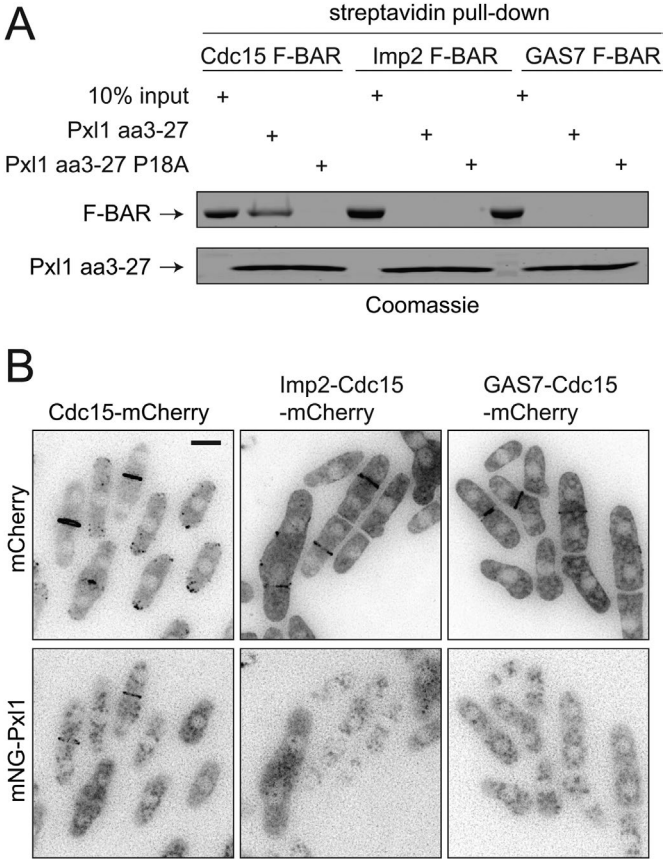

FIGURE 5: Pxl1 binds the Cdc15 F-BAR specifically. (A) Binding assay with biotinylated Pxl1 peptide (residues 3–27) and indicated F-BAR domains. Pxl1(3–27) P18A served as a negative control. Bound proteins were separated by SDS–PAGE and stained with Coomassie blue. One representative of two assays with the same results is shown. (B) Live-cell images of mNG-Pxl1 and the indicated F-BAR-Cdc15 chimeras tagged with mCherry. Deconvolved max projections are shown. Scale bar = 5 µm.

purified on a HiTrap Q SP anion exchange column (Cytiva Life Sciences) and Imp2 F-BAR domain on a HiTrap SP cation exchange column (Cytiva Life Sciences). F-BAR domains were then concentrated with Amicon Ultra Centrifugal Filters (EMD Millipore).

For MBP-Pxl1, 150 µM $ZnCl_2$ was added during the growth of the culture to log-phase. Frozen cell pellets were lysed in buffer 1 (20 mM Tris-HCl, pH 7.4, 150 mM NaCl, 1 mM DTT) with 200 µg/ml lysozyme (Sigma-Aldrich; L6876), cOmplete EDTA-free protease inhibitor cocktail (Roche; 05056489001), and 0.1% NP-40 (US Biologicals; N3500). Cell pellets were resuspended by continuous agitation on ice for 20 min. Lysates were then sonicated three times for 30 s, with at least a 30-s pause between sonications (Sonic Dismembrator Model F60, Fisher Scientific; power 15 W), and a clearing spin was done for 15–30 min at 10–13,000 rpm. Cleared lysate was added to amylose resin (New England Biolabs; E8021L) and allowed to nutate for 2 h at 4°C. Pxl1 bound resin was then washed three times for 5 min at 4°C with buffer 1, and then resuspended in buffer 1 to a 50% slurry. Protein concentration was calculated from Coomassie Brilliant Blue G (Sigma-Aldrich; B0770) stained SDS–PAGE-separated purified proteins with bovine serum albumin (BSA; Sigma-Aldrich; A9418) used as standards.

Frozen cell pellets of Flag-Cdc15 (E30K E152K) co-expressed with Pom1 were resuspended in buffer 2 (50 mM Tris, pH 7.4, 250 mM NaCl, 0.1% NP-40; US Biologicals; N3500) with the addition of 200 µg/ml lysozyme (Sigma-Aldrich; L6876), cOmplete EDTA-free protease inhibitor cocktail (Roche; 05056489001). Resuspended lysates were sonicated four times for 30 s, with a 30-s pause between sonications (Sonic Dismembrator Model F60, Fisher Scientific; power 15 W) followed by a clearing spin for 15 min at 13K rpm. Anti-FLAG(R) M2 Magnetic Beads (Millipore Sigma, M8823) washed in buffer 2 were incubated with the cleared lysate (100 µl packed volume of beads per 40 ml cleared lysate) for 2 h at 4°C. Beads were washed four times for 5 min at 4°C with buffer 2. Finally, Flag-Cdc15 (E30K E152K) was eluted with 500 µl of 50 mM Tris, pH 7.4, 250 mM NaCl, 200 µg/ml 3xFlag peptide (Sigma-Aldrich; F4799) and 5% BSA for 20 min in RT. The eluate was concentrated to 100 µl and a clearing spin was done for 15 min at 13K rpm in 4°C. Protein concentration was calculated from Coomassie Brilliant Blue G (Sigma-Aldrich; B0770) stained SDS–PAGE-separated purified proteins with BSA.

Binding assays

Binding assays with Cdc15 F-BAR domains and synthetic biotinylated Pxl1 or Cdc12 peptides (Genscript) were performed by mixing F-BAR domains at 0.05 µM and peptides at 0.10 µM with streptavidin UltraLink resin (Pierce; 17-5113-01) and incubating for 1 h at 4°C in buffer 2. After thorough washing, samples were separated by SDS–PAGE, then transferred to polyvinylidene difluoride (PVDF) membrane (Immobilon FL; EMD Millipore) for Western blotting. For detection of biotinylated peptides, a streptavidin IR dye was used for detection of biotinylated peptides (LI-COR Biosciences), anti-Cdc15 rabbit polyclonal antibody (VU326; Roberts-Galbraith *et al.*, 2009) for detection of Cdc15 F-BAR domains, and anti-GST polyclonal antibody for detection of GST-tagged Cdc15C. IR dye 680 and IR dye 800 secondary antibodies (LI-COR Biosciences) were used for detecting Cdc15 fragments. The blots were then scanned using an Odyssey CLx (LI-COR Biosciences). For Figure 5, the assay was performed similarly except for the following modifications: F-BAR domains were added at 0.5 µM and Pxl1 peptide at 0.5 µM and samples were analyzed by Coomassie blue staining after SDS–PAGE. For the quantitative binding curve in Figure 1E, Pxl1 (residues 3–27) or Cdc12 (residues 20–40) biotinylated peptides were incubated with 10 µl streptavidin UltraLink resin (Pierce) in varying concentrations from 0 to 25 µM peptide as indicated for 1 h with rocking at 4°C in 1 ml buffer 2. Beads were then washed twice with binding buffer. Cdc15 F-BAR domain (50 ng) was next added to the beads in binding buffer in a 50-µl total reaction volume. After incubation for 1 h with rocking at 4°C, the resin was pelleted by centrifugation and the supernatant was collected for analysis by SDS–PAGE and Western blotting. The quantity of Cdc15 F-BAR domain that remained unbound was quantified using the LI-COR ImageStudio software.

Binding assays with Cdc15 F-BAR domains and MBP/MBP-Pxl1, MBP-Pxl1 fragments, or MBP-Pxl1(P18A) were performed by mixing 1 µM MBP or MBP-Pxl1 on amylose resin with 5 µg Cdc15 F-BAR domain in buffer 2. Binding assays were incubated for 1 h at 4°C. Resin was then washed thoroughly and separated by SDS–PAGE. Gels were then stained with Coomassie blue and analyzed using an Odyssey CLx.

Binding assays of full-length Cdc15, Flag-Cdc15(E30K E152K) with MBP-tagged Pxl1 mutants (Pxl1 wild type, Pxl1[P18A], Pxl1[AxxA^6], Pxl1[P18A+AxxA^6] were done in buffer 2. Flag-Cdc15(E30KE152K) (0.5 µM) in a 50-µl binding reaction was subjected to phosphatase reaction for 15 min by adding $MnCl_2$ to a final concentration of 1 mM with 0.5 µl λ-phosphatase or buffer control. Next, the phosphatase-treated samples were added to

beads containing 0.5 μM of MBP-tagged Pxl1, Pxl1(P18A), Pxl1(AxxA^6), or Pxl1(P18A+ AxxA^6) and incubated for 1 h at 4°C. Beads were then washed five times in buffer 2. After the final wash, the buffer was removed and 30 μl 2X SDS–PAGE sample buffer was added. Samples were heated to 100°C and separated by freshly poured 8% Tris-glycine gels at 150 V for 2 h followed by transfer to PVDF membrane (Immobilon FL; EMD Millipore). Anti-Cdc15 rabbit polyclonal antibody (VU326; Roberts-Galbraith *et al.*, 2009) or anti-MBP mouse monoclonal antibody (E8032S; New England Biolabs) were used as primary antibodies in immunoblotting. Secondary antibodies were conjugated either to Alexa Fluor 680 or IRDye800 (LI-COR Biosciences). Immunoblots were visualized by using an Odyssey machine (LI-COR Biosciences).

Microscopy

Yeast for live-cell imaging were grown at 25°C. Live-cell images of *S. pombe* cells were acquired using a Personal DeltaVision (Cytiva Life Sciences, Marlborough, MA) that includes a microscope (IX71; Olympus), 60× NA 1.42 Plan Apochromat and 100× NA 1.40 U Plan S Apochromat objectives, fixed and live-cell filter wheels, a camera (either a Photometrics CoolSNAP HQ2 or a pco.edge 4.2 sCMOS), and softWoRx imaging software (Cytiva Life Sciences). Z sections were spaced at 0.5 μm. Images for quantification of CR intensity were not deconvolved and were sum projected. Intensity measurements were made with FIJI (Schindelin *et al.*, 2012).

For Pxl1 CR measurements, each measurement was corrected for background cell intensity. A region of interest was created to measure the intensity of the CR and background cell intensity was measured from a region in each cell used excluding the ring and the nucleus. The background cell intensity was subtracted from the CR measurements (Waters, 2009). For Figure 4, A and B, deconvolved sum projections were shown. Figure 5B images were deconvolved and max projected.

Time-lapse imaging was performed on log-phase cells using a CellASIC ONIX microfluidics perfusion system (Millipore Sigma, Burlington, MA). Cells were loaded into Y04C plates for 5 s at 8 psi, and YE liquid medium flowed into the chamber at 5 psi throughout the time-lapse. Images were acquired every 2 min with optical sections taken at 0.5-μm spacing. Time-lapse images were deconvolved with 10 iterations and visualized as maximum projections. In Supplemental Figure S1D cells were grown at 29°C.

For Supplemental Figure S3A, the events were defined as follows: "Formation" was the time from SPB separation to CR assembly. "Maturation" was the time from CR assembly to the onset of CR constriction. "Constriction" was the time from the first frame of CR constriction until the frame where the CR is completely constricted and has disassembled.

For Supplemental Figure S2A, cells were grown at 29°C and fixed with 70% ethanol. Cells were then stained with 4′,6-diamidino-2-phenylindole and methyl blue to visualize nuclei and septa.

Quantification and statistical analysis

Calculations of mean, standard error of the mean (SEM), and statistical significances were performed with Prism 8.0 (GraphPad Software). Significance was defined by a p value equal to or less than 0.05. One-way ANOVA was used with Tukey's post hoc test for multiple comparisons.

ACKNOWLEDGMENTS

We are grateful to Sierra Cullati and Tony Rossi for constructive comments on the manuscript. C.E.S. was supported by National Institutes of Health (NIH) Grant no. T32GM-00855421 and American Heart Association Grant no. 17PRE33410245. This work was supported by NIH Grant no. R35GM-131799 to K.L.G.

REFERENCES

Begonja AJ, Pluthero FG, Suphamungmee W, Giannini S, Christensen H, Leung R, Lo RW, Nakamura F, Lehman W, Plomann M, *et al.* (2015). FlnA binding to PACSIN2 F-BAR domain regulates membrane tubulation in megakaryocytes and platelets. Blood 126, 80–88.

Bhattacharjee R, Mangione MC, Wos M, Chen J-S, Snider CE, Roberts-Galbraith RH, McDonald NA, Presti LL, Martin SG, Gould KL (2020). DYRK kinase Pom1 drives F-BAR protein Cdc15 from the membrane to promote medial division. Mol Biol Cell 31, 917–929.

Cheffings TH, Burroughs NJ, Balasubramanian MK (2016). Actomyosin ring formation and tension generation in eukaryotic cytokinesis. Curr Biol 26, R719–R737.

Cortés JCG, Pujol N, Sato M, Pinar M, Ramos M, Belén M, Osumi M, Carlos RJ, Peréz P (2015). Cooperation between paxillin-like protein Pxl1 and glucan synthase Bgs1 is essential for actomyosin ring stability and septum formation in fission yeast. PLoS Genetics 11, 1–24.

Feng S, Chen JK, Yu H, Simon JA, Schreiber SL (1994). Two binding orientations for peptides to the Src SH3 domain: development of a general model for SH3-ligand interactions. Science 266, 1241–1247.

Garabedian MV, Stanishneva-Konovalova T, Lou C, Rands TJ, Pollard LW, Sokolova OS, Goode BL (2018). Integrated control of formin-mediated actin assembly by a stationary inhibitor and a mobile activator. J Cell Biol 217, 3512–3530.

Ge W, Balasubramanian MK (2008). Pxl1p, a paxillin-related protein, stabilizes the actomyosin ring during cytokinesis in fission yeast. Mol Biol Cell 19, 1680–1692.

Gould GW (2016). Animal cell cytokinesis: the role of dynamic changes in the plasma membrane proteome and lipidome. Sem Cell Dev Biol 53, 64–73.

Goyal A, Takaine M, Simanis V, Nakano K (2011). Dividing the spoils of growth and the cell cycle: the fission yeast as a model for the study of cytokinesis. Cytoskeleton 68, 69–88.

Kettenbach AN, Deng L, Wu Y, Baldissard S, Adamo ME, Gerber SA, Moseley JB (2015). Quantitative phosphoproteomics reveals pathways for coordination of cell growth and division by the conserved fission yeast kinase pom1. Mol Cell Proteomics 14, 1275–1287.

Kostan J, Salzer U, Orlova A, Toro I, Hodnik V, Senju Y, Zou J, Schreiner C, Steiner J, Merilainen J, *et al.* (2014). Direct interaction of actin filaments with F-BAR protein pacsin2. EMBO Rep 15, 1154–1162.

Liu Y, McDonald NA, Naegele SM, Gould KL, Wu JQ (2019). The F-BAR domain of Rga7 relies on a cooperative mechanism of membrane binding with a partner protein during fission yeast cytokinesis. Cell Rep 26, 2540–2548.e2544.

López-Colomé AM, Lee-Rivera I, Benavides-Hidalgo R, López E (2017). Paxillin: a crossroad in pathological cell migration. J Hematol Oncol 10, 50.

Lu Y, Sugiura R, Yada T, Cheng H, Sio SO, Shuntoh H, Kuno T (2002). Calcineurin is implicated in the regulation of the septation initiation network in fission yeast. Genes Cells 7, 1009–1019.

Mangione MC, Gould KL (2019). Molecular form and function of the cytokinetic ring. J Cell Sci 132, jcs226928.

Mangione MC, Snider CE, Gould KL (2019). The intrinsically disordered region of the cytokinetic F-BAR protein Cdc15 performs a unique essential function in maintenance of cytokinetic ring integrity. Mol Biol Cell 30, 2790–2801.

Martín-García R, Arribas V, Coll PM, Pinar M, Viana RA, Rincón SA, Correa-Bordes J, Ribas JC, Pérez P (2018). Paxillin-mediated recruitment of calcineurin to the contractile ring is required for the correct progression of cytokinesis in fission yeast. Cell Rep 25, 772–783.e774.

McDonald NA, Lind AL, Smith SE, Li R, Gould KL (2017). Nanoscale architecture of the *Schizosaccharomyces pombe* contractile ring. eLife 6, e28865.

McDonald NA, Vander Kooi CW, Ohi MD, Gould KL (2015). Oligomerization but not membrane bending underlies the function of certain F-BAR proteins in cell motility and cytokinesis. Dev Cell 35, 725–736.

Oh Y, Schreiter JH, Okada H, Wloka C, Okada S, Yan D, Duan X, Bi E (2017). Hof1 and Chs4 interact via F-BAR domain and Sel1-like repeats to control extracellular matrix deposition during cytokinesis. Curr Biol 27, 2878–2886.e2875.

Pinar M, Coll PM, Rincón SA, Pérez P (2008). *Schizosaccharomyces pombe* Pxl1 is a paxillin homologue that modulates Rho1 activity and participates in cytokinesis. Mol Biol Cell 19, 1727–1738.

Pollard TD, Wu J-Q (2010). Understanding cytokinesis: lessons from fission yeast. Nat Rev Mol Cell Biol 11, 149–155.
Ren L, Willet AH, Roberts-Galbraith RH, McDonald NA, Feoktistova A, Chen JS, Huang H, Guillen R, Boone C, Sidhu SS, *et al.* (2015). The Cdc15 and Imp2 SH3 domains cooperatively scaffold a network of proteins that redundantly ensure efficient cell division in fission yeast. Mol Biol Cell 26, 256–269.
Rincon SA, Paoletti A (2016). Molecular control of fission yeast cytokinesis. Semin Cell Dev Biol 53, 28–38.
Roberts-Galbraith RH, Chen J-S, Wang J, Gould KL (2009). The SH3 domains of two PCH family members cooperate in assembly of the *Schizosaccharomyces pombe* contractile ring. J Cell Biol 184, 113–127.
Roberts-Galbraith RH, Ohi MD, Ballif BA, Chen JS, McLeod I, McDonald WH, Gygi SP, Yates JR 3rd, Gould KL (2010). Dephosphorylation of F-BAR protein Cdc15 modulates its conformation and stimulates its scaffolding activity at the cell division site. Mol Cell 39, 86–99.
Schaller MD (2001). Paxillin: a focal adhesion-associated adaptor protein. Oncogene 20, 6459–6472.
Schindelin J, Arganda-Carreras I, Frise E, Kaynig V, Longair M, Pietzsch T, Preibisch S, Rueden C, Saalfeld S, Schmid B (2012). Fiji: an open-source platform for biological-image analysis. Nat Methods 9, 676.
Smith MA, Hoffman LM, Beckerle MC (2014). LIM proteins in actin cytoskeleton mechanoresponse. Trends Cell Biol 24, 575–583.
Snider CE, Chandra M, McDonald NA, Willet AH, Collier SE, Ohi MD, Jackson LP, Gould KL (2020). Opposite surfaces of the Cdc15 F-BAR domain create a membrane platform that coordinates cytoskeletal and signaling components for cytokinesis. Cell Rep 33, 108526.
Snider CE, Wan Mohamad Noor WNI, Nguyen NTH, Gould KL, Suetsugu S (2021). The state of F-BAR domains as membrane-bound oligomeric platforms. Trends Cell Biol 31, 644–655.
Stanishneva-Konovalova TB, Kelley CF, Eskin TL, Messelaar EM, Wasserman SA, Sokolova OS, Rodal AA (2016). Coordinated autoinhibition of F-BAR domain membrane binding and WASp activation by Nervous Wreck. Proc Natl Acad Sci USA 113, E5552–E5561.
Sun X, Phua DYZ, Axiotakis L Jr, Smith MA, Blankman E, Gong R, Cail RC, Espinosa de Los Reyes S, Beckerle MC, Waterman CM, Alushin GM (2020). Mechanosensing through direct binding of tensed F-actin by LIM domains. Dev Cell 55, 468–482.e467.
Teyra J, Huang H, Jain S, Guan X, Dong A, Liu Y, Tempel W, Min J, Tong Y, Kim PM, *et al.* (2017). Comprehensive analysis of the human SH3 domain family reveals a wide variety of non-canonical specificities. Structure 25, 1598–1610.e1593.
Turner CE (2000). Paxillin and focal adhesion signalling. Nat Cell Biol 2, E231–E236.
Waters JC (2009). Accuracy and precision in quantitative fluorescence microscopy. J Cell Biol 185, 1135–1148.
Willet AH, McDonald NA, Bohnert KA, Baird MA, Allen JR, Davidson MW, Gould KL (2015). The F-BAR Cdc15 promotes contractile ring formation through the direct recruitment of the formin Cdc12. J Cell Biol 208, 391–399.
Winkelman JD, Anderson CA, Suarez C, Kovar DR, Gardel ML (2020). Evolutionarily diverse LIM domain-containing proteins bind stressed actin filaments through a conserved mechanism. Proc Natl Acad Sci USA 117, 25532–25542.
Wood V, Harris MA, McDowall MD, Rutherford K, Vaughan BW, Staines DM, Aslett M, Lock A, Bähler J, Kersey PJ (2012). PomBase: a comprehensive online resource for fission yeast. Nucleic Acids Res 40, D695–D699.
Wu JQ, Pollard TD (2005). Counting cytokinesis proteins globally and locally in fission yeast. Science 310, 310–314.
Yao G, Su X, Nguyen V, Roberts K, Li X, Takakura A, Plomann M, Zhou J (2014). Polycystin-1 regulates actin cytoskeleton organization and directional cell migration through a novel PC1-Pacsin 2-N-Wasp complex. Hum Mol Genet 23, 2769–2779.
Yoshida T, Toda T, Yanagida M (1994). A calcineurin-like gene ppb1+ in fission yeast: mutant defects in cytokinesis, cell polarity, mating and spindle pole body positioning. J Cell Sci 107(Pt 7), 1725–1735.
Yu H, Chen JK, Feng S, Dalgarno DC, Brauer AW, Schreiber SL (1994). Structural basis for the binding of proline-rich peptides to SH3 domains. Cell 76, 933–945.